Research Square

Preprints are preliminary reports that have not undergone peer review.
They should not be considered conclusive, used to inform clinical practice,
or referenced by the media as validated information.

Pyrolysis-Based Fire Modeling of Polyurethane Foam Incorporating a Grid-Independent Method

Taehoon Kim

tkim@seoultech.ac.kr

Seoul National University of Science and Technology

Research Article

Keywords: Fire modeling, Fire simulation, Grid sensitivity, Polyurethane foam, Pyrolysis

Posted Date: November 6th, 2026

DOI: https://doi.org/10.21203/rs.3.rs-11425033/v1

License: This work is licensed under a Creative Commons Attribution 4.0 International License.
Read Full License

Additional Declarations: No competing interests reported.

Pyrolysis-Based Fire Modeling of Polyurethane Foam Incorporating a Grid-Independent Method

Taehoon Kim[a*]

[a] Department of Safety Engineering, Seoul National University of Science and Technology, 232 Gongneung-ro, Nowon-gu, Seoul 01811, Republic of Korea

Corresponding author

Taehoon Kim, Ph.D.

Associate Professor
Department of Safety Engineering,
Seoul National University of Science and Technology,
232 Gongneung-ro, Nowon-gu, Seoul 01811, Republic of Korea
Tel: +82-2-970-6374
E-mail: tkim@seoultech.ac.kr

ORCiD: 0000-0003-4113-8770

Abstract

To apply pyrolysis-based fire modeling to fire risk assessment, problems associated with coarse grids, such as inaccurate predictions of ignition and fire spread, must be addressed. Polyurethane foam (PUF) is widely used as an insulating material, and its constituent components are well characterized, making it suitable for pyrolysis-based fire modeling. In this study, a PUF fire model was developed using a pyrolysis model incorporating a grid-independent modeling method. PUF was represented by three components: virgin polyurethane foam, polyol beads, and a polyol layer. The combustion characteristics were adjusted by varying the area exposed to gas-phase cells and validated against cone calorimeter experiments. The proposed PUF fire model smoothly reproduced the two-stage combustion behavior, although the peak heat release rate during the second stage was overpredicted, particularly at low external radiative heat fluxes. Based on the validated PUF fire model, the grid-independent method was applied to PUF slab fire simulations. The method adjusted thermal properties and reaction kinetic parameters according to the cell temperature, which varied with grid size, while maintaining the one-dimensional heat transfer solution. The proposed method successfully reproduced the HRR and fire spread rate of the PUF slab fire, although a time delay in fire development was observed.

43 # Keywords

44 Fire modeling, Fire simulation, Grid sensitivity, Polyurethane foam, Pyrolysis

45

NOMENCLATURE

A	Pre-exponential factor for the solid phase reaction ($s^{-1}(kg/m^3)^{1-n_s}$)
c_p	Specific heat (J/(kg·K))
D^*	Characteristic fire diameter (-)
E_a	Activation energy (J/mol)
g	Gravitational acceleration (m/s^2)
h_r	Heat of reaction (J/kg)
k	Thermal conductivity (W/(m·K))
n_s	Reaction order
$\dot{Q}$	Heat release rate (kW)
R	Universal gas constant (8.314 J/(mol·K))
T_g	Gas phase temperature (K)
T_s	Solid phase temperature (K)
T_∞	Ambient temperature (K)
t	Time (s)
x	Depth (m)

Greek symbols

δ	Thickness (m)
ρ	Solid density (kg/m^3)
ρ_∞	Ambient air density (kg/m^3)

ABBREVIATIONS

AF	Area fraction
CFD	Computation fluid dynamics
DNS	Direct numerical simulation
HRR	Heat release rate
HRRPUA	Heat release rate per unit area
LES	Large eddy simulation
MF	Mass fraction
PUF	Polyurethane foam
TC	Thermocouple
vPUF	Virgin polyurethane foam

1. Introduction

Fire simulation is widely used in the field of fire safety for application such as fire risk assessment, evacuation safety analysis, and performance-based design. The most common approach in these applications is to use a design fire, which represents the fire growth and the maximum heat release rate (HRR) using an artificial burner. When applied to appropriate cases, such as over-ventilated fires and fires with constant products yields, this approach is useful despite its simplicity. However, to extend the application of fire simulation to a wider range of scenarios, the underlying physics of fire development should be considered.

One approach to incorporating the underlying physics is to use a pyrolysis model in fire simulations. This approach enables the effects of heat feedback to the fuel surface to be calculated. Polyurethane foam (PUF) is an effective material for applying pyrolysis models because its solid-phase components are well characterized, allowing its thermal properties and reaction kinetics to be specified. PUF is widely used as an insulating material in buildings [1] and furniture [2], but it is highly susceptible to fire. For these reasons, PUF has been the subject of numerous previous studies on pyrolysis modeling.

When the PUF catches on fire, it undergoes low-temperature pyrolysis, producing combustible gases and solid polyol. As the solid temperature increases, the polyol undergoes pyrolysis at a higher temperature, producing additional combustible gas. Based on this phenomenon, two approaches have been adopted in previous studies: the layering approach and the mixture approach. The layering approach was first proposed by Prasad et al. [3] to reproduce the two-stage combustion characteristics of PUF. They considered two components: virgin polyurethane foam (vPUF) and polyol, with each component represented as a separate layer. Two reactions were adopted for each component. However, this approach could not reproduce a smooth transition from the first stage to the second stage. McKeen and Liao [4] proposed a method in which the two components (vPUF and polyol) were mixed to modify the thermal properties of the bottom layer and reduce the thermal inertia. Using this method, the two-stage combustion was smoothly connected. Chen et al. [5] adopted five components: vPUF, polyol, carbodiimide, polycarbodiimide, and residue. The first layer was composed of vPUF, which produces

combustible gas. The second layer, initially composed of vPUF, produced combustion gas and solid products that were subsequently converted to polyol and carbodiimide. The produced carbodiimide was then converted into polycarbodiimide and residue, sequentially producing combustible gas. Most previous studies have been based on the layering approach, whereas Pau [6] used the mixture approach. Various methods were examined, and the final model adopted the mixture approach. In this approach, vPUF was represented as a mixture with thermal properties between those of vPUF and polyol.

Although the many researchers investigated PUF modeling methods using pyrolysis models, two issues remain. First, previous pyrolysis-based PUF fire models did not account for physical phenomena observed in experiments, such as bead formation on the vPUF surface [4, 7, 3]. Second, pyrolysis-based fire modeling is highly dependent on grid size and is difficult to apply with coarse grids. This limitation restricts the application of pyrolysis-based fire models to fire risk assessment.

Prasad et al. [3] conducted PUF slab fire simulation using a pyrolysis-based fire model. However, a grid size as small as 1 mm was used, while the simulation domain was 1.2 m × 1.2 m × 1.0 m. To reduce the computational cost, an anisotropic grid was used, which is not appropriate for Large Eddy Simulation (LES) because resolving large-scale turbulent vortices requires sufficient spatial resolution in all direction. Mangs and Hostikka [8] used 0.5-mm grid to analyze vertical fire spread over a birch rod using Direct Numerical Simulation (DNS). They found that the flame-spread characteristics obtained using a 0.5-mm grid were practically identical to those obtained using a 1.0-mm grid. However, this conclusion was limited to concurrent-flow flame spread, in which the flame is tilted in the direction of flame spread and heat transfer ahead of the pyrolysis front relatively effective. In the case of opposed-flow flame spread, a smaller grid size is expected to be required to obtain a grid-independent results. Most studies that successfully analyzed fire using pyrolysis models without modifying the reaction parameters employed grid sizes on the order of 1–10mm [9-11], depending on the heat feedback and flow characteristics.

The used of grid sizes on the order of 1–10 mm restricts the application of fire simulations to practical scenarios and requires substantial computational resources. For this reason, relatively coarse grids are

generally used in practical fire simulations. In the field of pyrolysis-based fire modeling, grid sizes on the order of 20–200 mm are commonly used. Dréan et al. [12] investigated fire spread over cladding using 20-mm gird, while Cui et al. [13] investigated a timber building fire using a 200-mm grid. The problem with pyrolysis-based fire simulation using coarse grids is that ignition and fire-spread characteristics can be inaccurately predicted when the fire is not sufficiently large to provide adequate heat feedback to the fuel surface [14].

In this study, a PUF fire model based on experimentally observed physical phenomena was proposed. In addition, a grid-independent fire modeling method was developed to enable the application of the PUF fire model to PUF slab fires using relatively coarse grid on the order of 20 to 50 mm. To compare the simulation results with experimental data, the experimental data reported by Pau [6] were selected. This study was selected because it provides the thermal properties and reaction kinetic parameters of the test material. In addition, the experiments progressed from cone calorimeter tests to PUF slab fire tests, which were sequentially required for the validation conducted in this study. However, the original reference is a dissertation. Therefore, the corresponding journal publication was sought and cited instead where available. Fire Dynamics Simulator (FDS) v6.9.1 was used for all the simulation results in this study.

2. Simulation Methodology

A polyurethane foam fire was reproduced using a pyrolysis model. To apply this model to large-scale fire simulations, a method for reducing grid-dependent characteristics was proposed. For clarity, the grid-independent fire modeling method used in this study is introduced first, followed by and explanation of the polyurethane foam fire model based on pyrolysis.

2.1 Grid-Independent Fire Modeling Method

Maragkos and Merci [15] reported that the flame near the fuel surface becomes smeared when a coarse grid is used. This can prevent accurate prediction of radiative emission. Furthermore, even if the radiation emission is accurately predicted, the incident heat flux still be affected by the grid size. Fig. 1 illustrates an example of the incident radiative heat flux ahead of a flame. The incident heat flux at the first cell in the fine-grid case is normalized to unity, and theoretical incident heat flux is assumed to decrease in proportion to the inverse square of the distance from the burning cell. If the critical heat flux for ignition is assumed to be 0.4, the cell adjacent to the burning cell can be ignited in the fine-grid case. However, as the grid becomes coarser as in Fig. 1 (b), the incident radiative heat flux at the adjacent to the burning cell falls below the critical heat flux, even when the theoretical heat-flux distribution is predicted. This demonstrates the grid-dependent nature of fire spread predictions, regardless of the accuracy of the radiation, combustion, or pyrolysis models. To mitigate this grid dependency in predicting flame spread —which must be accurately modeled to predict the HRR—this study proposes a method for modifying the properties governing fire spread according to grid size. The one-dimensional heat-transfer equation for a solid phase cell is given by

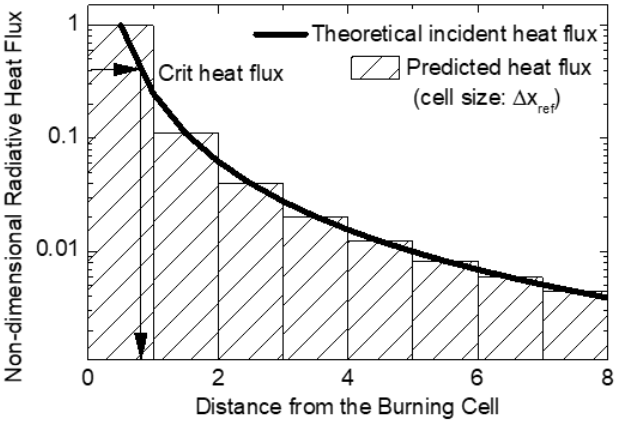
$$\rho c_p \frac{\partial T_s}{\partial t} = k \frac{\partial^2 T_s}{\partial x^2} + A\rho^{n_s} exp\left(-\frac{E_a}{RT_s}\right) h_r. \quad (1)$$

Here, ρ is the solid density (kg/m^3), c_p is the specific heat (J/(kg·K)), T_s is the temperature inside the solid (K), k is the thermal conductivity (W/(m·K)), x is the depth (m), A is the pre-exponential factor ($s^{-1}(kg/m^3)^{1-n_s}$), n_s is the reaction order, E_a is the activation energy (J/mol), R is the universal gas constant (8.314 J/(mol·K)), and h_r is the heat of reaction (J/kg). The last term represents the heat released or absorbed by the solid-phase reaction. Even at the same HRR, the incident heat flux received by the adjacent cell differs depending on the mesh resolution, resulting in lower temperature for the coarse mesh. To maintain the fire spread characteristics even on a coarse mesh, the pyrolysis reaction must occur at an incident heat flux below the critical heat flux. The most common approach to overcome this issue is to revise the kinetic constants (A and E_a). In this study, a method for correcting the activation energy based on the Arrhenius number is proposed. Currently, a common approach to reducing grid-size dependency is to exploit well-established physical phenomena [16] or dimensionless numbers [17]. This modification directly affects internal solid heat transfer, as it alters the final term of Eq. (1). Therefore, maintaining these heat transfer characteristics inside the solid is essential. Adjusting activation energy (E_a) depends on the grid size; more precisely, it is driven by how the temperature predictions vary with grid resolution. It was assumed that if the Arrhenius number (E_a/T_s) is preserved regardless of grid size, the flame spread rate will also be maintained. Since the solid phase temperature is difficult to measure directly while modifying activation energy (E_a), it was assumed that the solid temperature variance across grid sizes is proportional to the gas-phase temperature (T_g). Consequently, the maximum gas phase temperature was measured to determine the appropriate activation energy (E_a) for each grid size while keeping the Arrhenius number constant. To preserve the same heat transfer characteristics within the solid-phase cell under Arrhenius similarity, Eq. (1) was reformulated by introducing $\Theta = T_s/E_a$, yielding the following revised heat transfer equation:

$$\rho c_p \frac{\partial \Theta}{\partial t} = k \frac{\partial^2 \Theta}{\partial x^2} + \frac{A}{E_a} \rho^{n_s} exp\left(-\frac{1}{R\Theta}\right) h_r. \quad (2)$$

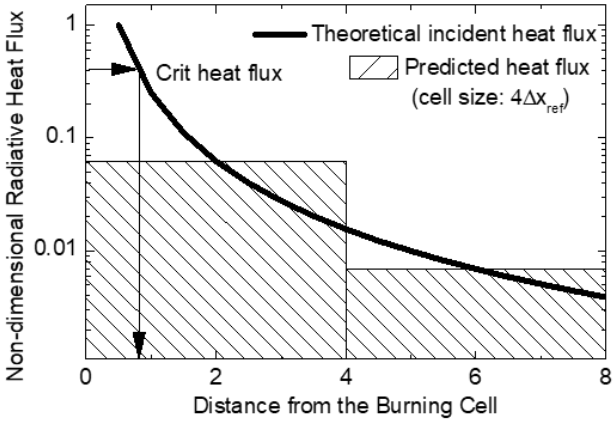
To maintain the solid-phase heat transfer characteristics regardless of grid size, the three terms (ρc_p, k, and $(A/E_a)\rho^{n_s}$) in Eq. (2) and the Arrhenius number (T_s/E_a) must remain invariant.

198



199

200 (a)



201

202 (b)

203 **Fig. 1** Incident radiative heat flux depending on the grid size: (a) Fine grid size case and (b) Coarse

204 grid size case

205

2.2 Polyurethane Foam Fire Modeling

2.2.1 Solid Phase Modeling

The most common and simple approach for modeling polyurethane foam pyrolysis is a two-step pyrolysis model [18-21]. Based on observations from previous studies, these two stages progress as shown in Fig. 2 (a). Initially, vPUF decomposes into a higher-density polyol while releasing pyrolysis gas. The generated polyol forms small beads on the surface of virgin polyurethane foam [22, 7, 3, 5]. In the first stage, the pyrolysis gases are generated from both vPUF and the resulting polyol. As the thermal degradation proceeds into the second stage, this polyol forms a layer and produce pyrolysis gas [23]. Current fire simulation tools cannot explicitly model this physical transformation (i.e, polyol bead generation and polyol layer formation). Therefore, three seperate vPUF obstructions were defined: one producing pyrolysis gas (vPUF1), another generating polyol beads (vPUF2), and the last creating the polyol layer (vPUF3). Their ratios were adjusted using the 'AREA_MULTIPLIER' parameter, decoupled from the geometrical area exposed to the gas-phase cells. Since the area supplying pyrolysis gas into the gas-phase cells changes with the 'AREA_MULTIPLIER', the density of the vPUF obstruction was adjusted to conserve fuel mass. Based on this approach, two modeling methods were evaluated: one without the 'BURN_AWAY' option and the other with it. When the 'BURN_AWAY' option is not used, the obstruction retains its original geometry. Consequently, the vPUF generating the polyol layer must be present at the start of simulation. To prevent heat transfer and combustion during the first stage, a thin incombustible obstruction was placed over the layer composed of vPUF3, which transforms into polyol layer. This thermal barrier was set to disappear when the mass of vPUF1 in adjacent cell decreased to 5% of its initial mass. This approach was used to analyze the combustion characteristics of PUF in a cone calorimeter test. When 'BURN_AWAY' option is used, the vPUF obstructions generating pyrolysis gas and polyol beads (vPUF1 and vPUF2, respectively) were placed on top of vPUF3, which transforms into the polyol layer. To align its surface with the height of the burning polyol layer, vPUF3 was positioned one cell layer below the physical thickness of the actual PUF. Since the second method utilizes 'BURN_AWAY' option, it can capture changes in the burning

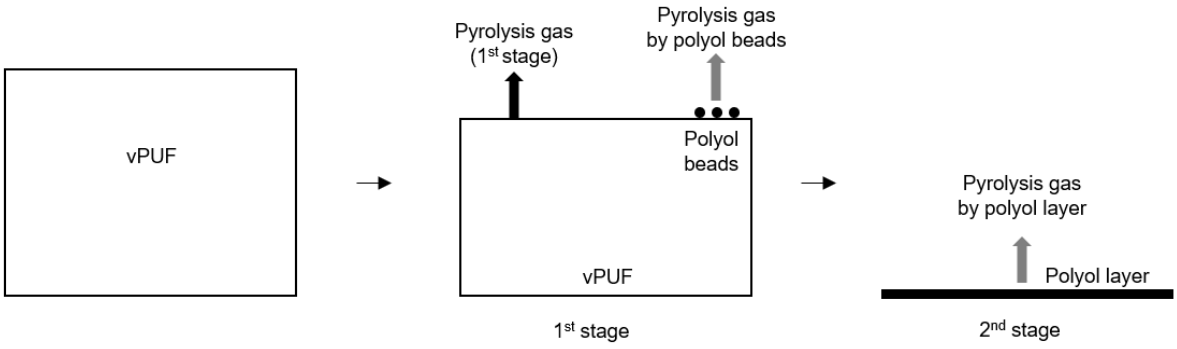
area—and consequently the variation in heat absorption and fuel release—as the fire develops. In Method 2, grid-independent model discussed in the previous section was also adopted. This approach was used to analyze the fire behavior of a PUF slab. Regardless of the methods, solid phase reaction kinetics are as follows:

$$vPUF1 \rightarrow Pyrolysis\ gas1 \tag{3}$$

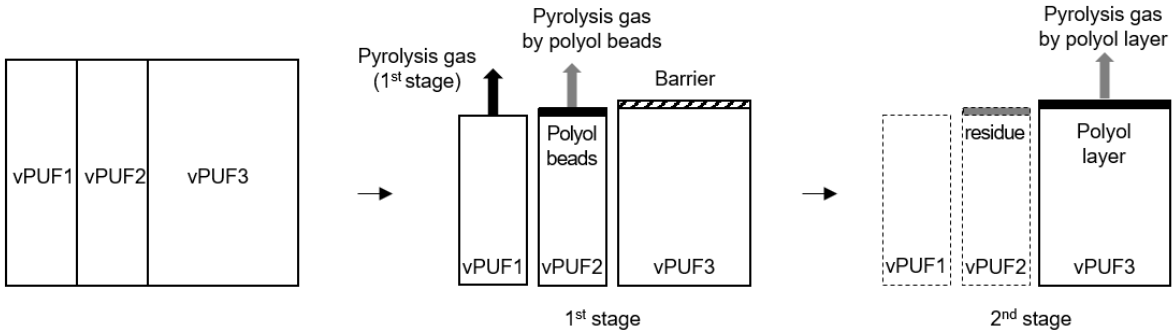
$$vPUF2 \rightarrow Polyol\ bead \rightarrow 0.973 Pyrolysis\ gas2 + 0.027 residue \tag{4}$$

$$vPUF3 \rightarrow Polyol\ layer \rightarrow 0.973 Pyrolysis\ gas2 + 0.027 residue \tag{5}$$

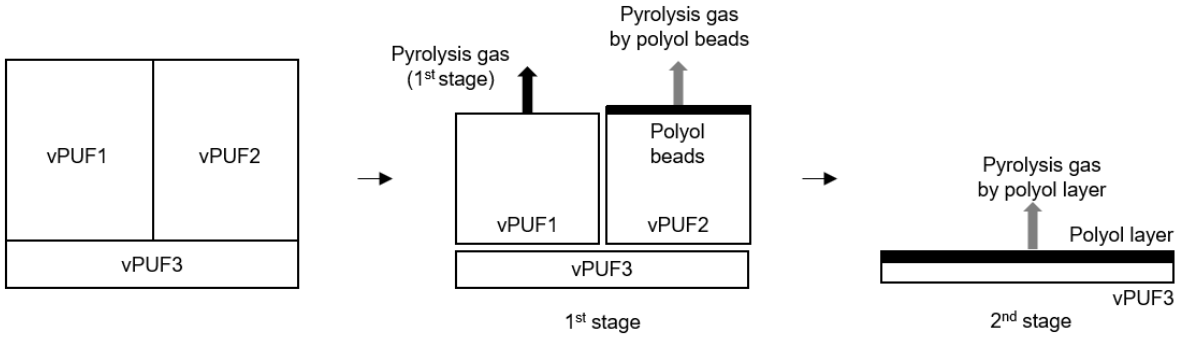
Since vPUF2 and vPUF3 have different 'AREA_MULTIPLIER' values—and consequently different densities—the solid vPUF had to be defined separately. However, their gaseous phase transformations were set identically because they consist of the same material. In addition, the residue was configured with properties identical to polyol, with its quantity set to match the remaining mass observed in the TGA results by Pau [6]. The concepts of the PUF fire model for two methods are illustrated in Fig. 2 (b) and (c)



(a)



(b)



(c)

Fig. 2 Burning process of the polyurethane foam fire and modeling methods: (a) Burning process of the polyurethane foam, (b) First method ('BURN_AWAY=F'), and (c) Second method ('BURN_AWAY=T' and with grid-independent model)

Table 1 summarizes the base thermal properties and kinetic constants used in this study. The thermal properties were adopted from the previous study by Pau [6, 24]. It is known that vPUF produces 26 wt% gaseous products, while the remaining 74 wt% is converted into polyol [21]. The solid polyol subsequently undergoes pyrolysis at higher temperatures, producing gaseous products and solid residue [6, 25]. The heat of reaction is generally defined on the basis of the reactant, which in this case is vPUF. However, the present study considers two parallel pyrolysis pathways of vPUF: one producing low-temperature gaseous pyrolysis products and the other forming solid polyol. Because each pathway generates a different pyrolysate, the heat of reaction was defined on the basis of the corresponding

gaseous pyrolysis products. The values used in this study were obtained from the previous TGA experiment by Pau [6, 25]. Additionally, for the same reason, the kinetic constants for the pyrolysis reaction were recalculated using a "Model free" method [26].

Table 1. Base thermal properties and kinetic constants of vPUF and polyol [6, 25, 24] (Kinetic constants were recalculated according to the definitions used in this study).

	vPUF	Polyol
Density (kg/m^3)	31	1019
Specific heat (kJ/kg·K)	2.996	2.053
Conductivity (W/m·K)	0.049	0.186
Heat of Reaction (kJ/kg)	891	233
A ($s^{-1}(kg/m^3)^{1-n_s}$)	4.02×10^{14}	7.38×10^{15}
E_a (kJ/mol)	179	231
n_s	1.35	1.25

As illustrated in Fig. 2, the PUF was composed of three obstructions (vPUF1, vPUF2, and vPUF3). For this purpose, four cells were chosen as a unit obstruction representing the PUF. When using Method 1, all component obstructions (vPUF1, vPUF2, and vPUF3) are exposed to the gas cell. Since the adjustment of the geometric area fraction exposed to the gas cell is restricted, 'AREA_MULTIPLIER' was adopted and its value was adjusted by comparing the HRR with experimental data. In Method 2, vPUF3, which transforms into a polyol layer, is located under vPUF1 and vPUF2; thus, its geometric area fraction is 1.0. To maintain the same area in both methods, 'AREA_MULTIPLIER' was set accordingly. The polyol bead burns in the first stage, and its exposed area is reduced as bead form. Therefore, the area fraction of vPUF2 was set relatively lower than that of vPUF3. In addition to the area fraction, the mass fraction of each component was adjusted. Since vPUF1 represents the pyrolysis gas produced from the low-temperature pyrolysis reaction and its amount is fixed, its area fraction and the mass fraction were fixed to the ratio observed in the TGA experiment (26 %). By adjusting the mass fractions of vPUF2 and vPUF3, the amount of heat released during the first and the second stage combustion can be adjusted. Similar to 'AREA_MULTIPLIER', the mass fraction was also adjusted by

285 comparing it with the experiment HRR data. The parameters determined based on experimental
286 observations are marked with an asterisk (*) in Table 2.

287

288 **Table 2.** Geometrical parameters used for the PUF fire model.

		vPUF1	vPUF2 (Polyol bead)	vPUF3 (Polyol layer)
Method 1	Area Multiplier	1.04*	0.4	1.0
	Geometric Area Fraction	0.25	0.25	0.5
Method 2	Area Multiplier	0.52*	0.2	0.5
	Geometric Area Fraction	0.5	0.5	1.0
Area Fraction		0.26*	0.1	0.5
Mass Fraction		0.26*	0.222(0.3)	0.518(0.7)

289

290

Based on the thermal properties and kinetic constants summarized in Table 1, the parameters of the grid-independent PUF fire model were calculated using the method described in Section 2.1, as summarized in Table 3. The mass fraction and the area fraction of each component were set as in Table 2; therefore, the modeled thickness (δ_{model}) in Table 3 can be caclulated. In this study, the maximum temerapture ($T_{max,\Delta x}$) was predicted by extrapolating the cone calorimeter simulation results, while the reference temperature (T_{ref}) was set to the adiabatic flame temperature.

The heat transfer within the solid phase is calculated using a one-dimensional heat transfer equation. This calculation is performed using one-dimensional cells in the solid phase, extending from the solid surface toward the backside of the solid. The solid phase cell size was calulated as $\sqrt{k/\rho c_p}$ and uniformly distributed throughout the pyrolyzing solid. For non-pyrolyzing solids, the solid-phase cells were generated by successively doubling the cel size from the surface toward the center of the solid, followed by successively halving the cell size from the center toward the backside. This follows the default solid-phase cell distribution in FDS.

Table 3. Thermal properties and kinetic constants used for the PUF fire model.

	vPUF1	vPUF2	Polyol bead	vPUF3	Polyol layer
Density (kg/m^3)	ρ_{vPUF}	$\rho_{vPUF}\frac{MF}{AF}\frac{\delta_{actual}}{\delta_{model}}$	ρ_{polyol}	$\rho_{vPUF}\frac{MF}{AF}\frac{\delta_{actual}}{\delta_{model}}$	ρ_{polyol}
Specific heat (J/kg·K)	$c_{p,vPUF}$	$c_{p,vPUF}\frac{\rho_{vPUF}}{\rho_{vPUF2}}$	$c_{p,polyol}$	$c_{p,vPUF}\frac{\rho_{vPUF}}{\rho_{vPUF3}}$	$c_{p,polyol}$
Conductivity (W/m·K)	k_{vPUF}	k_{vPUF}	k_{polyol}	k_{vPUF}	k_{polyol}
A ($s^{-1}(kg/m^3)^{1-n_s}$)	$A_{vPUF}\frac{E_{a,vPUF1}}{E_{a,vPUF}}$	$A_{vPUF}\frac{E_{a,vPUF2}}{E_{a,vPUF}}\frac{\rho_{vPUF}{}^{n_s}}{\rho_{vPUF2}{}^{n_s}}$	$A_{polyol}\frac{E_{a,polyol\ bead}}{E_{a,polyol}}$	$A_{vPUF}\frac{E_{a,vPUF3}}{E_{a,vPUF}}\frac{\rho_{vPUF}{}^{n_s}}{\rho_{vPUF3}{}^{n_s}}$	$A_{polyol}\frac{E_{a,polyol\ bead}}{E_{a,polyol}}$
E_a (J/mol)	$E_{a,vPUF}\frac{T_{ref}}{T_{max,\Delta x}}$	$E_{a,vPUF}\frac{T_{ref}}{T_{max,\Delta x}}$	$E_{a,polyol}\frac{T_{ref}}{T_{max,\Delta x}}$	$E_{a,vPUF}\frac{T_{ref}}{T_{max,\Delta x}}$	$E_{a,polyol}\frac{T_{ref}}{T_{max,\Delta x}}$

2.2.2 Gas Phase Modeling

The gas phase of the PUF was modeled using the method proposed by Chen et al. [5]. In this model, the gas produced by the low-temperature pyrolysis reaction, designated as 'Pyrolysis gas1' in this study, was represented by $C_9H_6N_2O_2$, while the gas produced by the high-temperature pyrolysis reaction, designated as 'Pyrolysis gas2', was represented by $C_6H_{14}O_3$. Air was modeled as a lumped species consisting of nitrogen, oxygen, carbon dioxide, and water vapor, while the combustion products were modeled as a lumped species consisting of nitrogen, carbon monoxide, carbon dioxide, water vapor, and soot. The heat of combustion for 'Pyrolysis gas1' and 'Pyrolysis gas2' were set to 24 and 28 kJ/kg respectively [21]. The Eddy Dissipation Concept combustion model was used for predicting change in species concentration. Gas phase suppression ('SUPPRESSION') was turned off because the cell size used in this study was relatively coarse, making it difficult to accurately predict the extinction temperature. In addition, the flame extinction was beyond the scope of this study.

By defaults, FDS calculates radiative heat transfer by assuming that the gas phase behaves as a gray gas and using a single absorption coefficient in the radiative heat transfer equation (RTE). FDS also supports improved absorption coefficient model that accounts for the dependence of gas radiation on the wavelength and the participating species. Ahmed and Trouvé [27] investigated thermal feedback in a medium-scale methanol pool fire and reported that the Weighted Sum of Gray Gases (WSGG) model predicted higher radiative heat feedback to the fuel surface near the flame boundary. This effect is particularly important in fire simulations involving pyrolysis reactions, as the results are highly sensitive to the surface temperature. For this reason, WSGG model was used in this study. The grid size used in the fire simulation is usually much larger than the length scale of the flame structure. In addition, the production and oxidation of soot, which plays a dominant role in radiative heat transfer, are not explicitly resolved in the fire simulation. As a result, the radiative emission by the flame cannot be accurately predicted. For this reason, FDS employs prescribed radiative fraction. For common combustible materials that produce sooting flames, the radiative fraction typically ranges from 0.3 to 0.4. In this study, a value of 0.35 was used. To achieve this radiative fraction, the calculated radiation

emission source term is corrected by a factor of up to 100 times its original value. However, in FDS v6.9.1, which was used in this study, the correction factor is not allowed to fall below unity. In this study, the minimum correction factor 'C_MIN' was reduced from the default value of 1.0 to 0.1. This setting is consistent with that of the latest version of FDS (v6.11.1).

3. Simulation Conditions

The methods described in Section 2 were used for the simulation-experiment comparison. The first case was based on a cone calorimeter experiment following ISO 5660, while the second case involved a PUF slab fire. The experimental conditions and corresponding data for both cases were adopted from the study by Pau [6]. This study was selected because it employed a sequential approach, progressing from a small-scale fire experiment to a large-scale fire test using the same material, for which the thermal properties were also provided.

3.1 Cone Calorimeter Fire Simulation Conditions

Based on the cone calorimeter test method [28], the cone heater and PUF specimen were reproduced in the simulation domain. In the simulation, only the top surface was modeled as a PUF surface of which size is 0.1×0.1 m^2 considering that the sides of the specimen were covered with aluminum foil during the test. In PUF modeling method 1, each material (vPUF1, vPUF2, and vPUF3) were directly exposed to the gas-phase cells. An 18-mm-thick calcium silicate board layer was placed beneath each of vPUF1, vPUF2, and vPUF3 layers. In PUF modeling method 2, vPUF1 and vPUF2 were initially exposed to the gas-phase cells. As these materials burned, vPUF3, which constituted the final cell layer, was subsequently exposed to the gas-phase. Therefore, an 18- mm-thick calcium silicate board layer was placed beneath the vPUF3 layer. In both methods, the original PUF thickness was set to 50 mm. The thermal boundary condition at the backside of the specimen was set to 'VOID', meaning that the backside was exposed to the fictitious air region in the FDS.

The cone heater geometry was reproduced for each grid size to minimize the geometrical discrepancy between the simulation model and the actual experimental configuration. The coil surface temperature was adjusted to achieve the target heat flux at the specimen surface. The target heat flux ranged from

30 to 60 kW/m^2 in increments of 10 kW/m^2. The target heat fluxes and corresponding coil temperatures are summarized in Table 4.

Table 4. Base thermal properties and kinetic constants of vPUF and polyol.

Coil temperature (°C)		Target heat flux (kW/m^2)			
		30	40	50	60
Grid Size (mm)	5	656	729	784	834
	6.25	663	733	791	839
	8.33	671	742	801	852

In this study, three grid sizes (5, 6.25, and 8.33 mm) were considered. The Plume Resolution Index (PRI) [29] was calculated as a characteristic fire diameter (Q^*) [30] divided by the grid size (Δx). A characteristic fire diameter was calculated by

$$Q^* = \left(\frac{\dot{Q}}{\rho_\infty c_{p,air} T_\infty \sqrt{g}}\right)^{0.4}. \quad (6)$$

Here, $\dot{Q}$ is the heat release rate of the fire (kW), ρ_∞ is the ambient density (kg/m^3), $c_{p,air}$ is the specific heat of the ambient air (J/(kg·K)), T_∞ is the ambient temperature (K), and g is the gravitational acceleration (m/s^2). The PRI values corresponding to the grid sizes of 5, 6.25, and 8.33 mm used in this study were 30.3, 24.3, and 18.2, respectively. The simulation domain for the cone calorimeter fire simulation is depicted in Fig. 3. The horizontal domain size varies from 24 to 30 cm, while the vertical distance from the PUF surface to the top of the domain varies from 73.5 to 80 cm, depending on the grid size. The vertical distance from the bottom of the domain to the top surface of the PUF was fixed to 7.5 cm. The bottom of the domain was left open to minimize flow interference and allow unobstructed air entrainment into the domain.

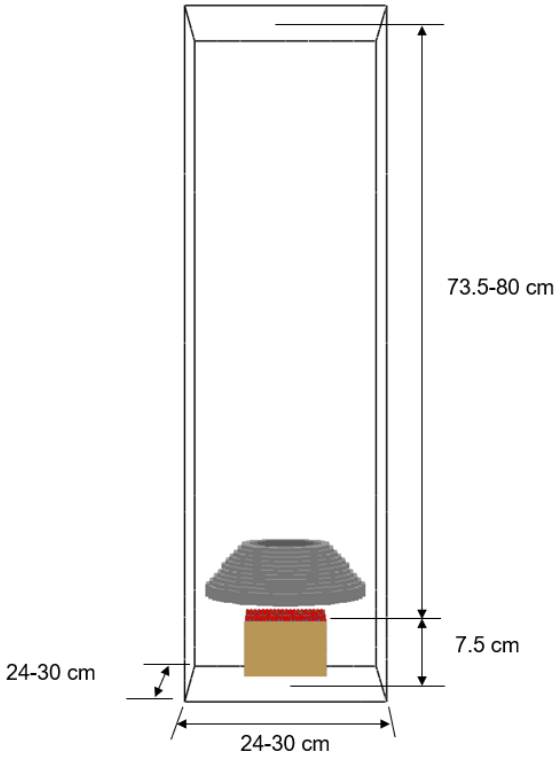


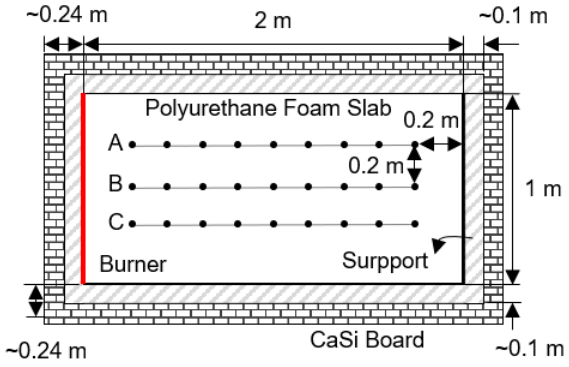
Fig. 3 Simulation domain for cone calorimeter fire simulation

3.2 Polyurethane Foam Slab Fire Simulation Conditions

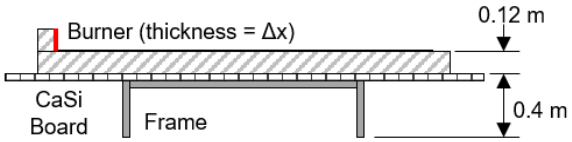
The PUF slab fire simulation was carried out using the same setup as that reported by Pau [6] and presented in Fig. 4. A 1 m × 2 m PUF slab with a thickness of 120 mm was placed on a calcium silicate board, and the sides of the slab were surrounded by support bracing. The detailed dimension of the support structure were not reported in the previous work by Pau [6]. Therefore, the dimensions and properties of the supporting materials were assumed in this study. The support structure had an estimated thickness of 0.24 m, although its actual thickness varied depending on the grid size. The support consisted of a 12-mm-thick calcium silicate board and 100-mm-thick timber. The thermocouple (TC) array was placed on the PUF slab at 0.2 m intervals, following the arrangement used by Pau [6].

The PUF slab, support structure, and calcium silicate board were placed on a frame to reproduce the ambient gas flow conditions of the experiment. The burner used in the experiment consisted of regularly

spaced apertures. However, the aperture size was too small to be resolved in the simulation. Therefore, the burner was modeled with a height of one cell along one side of the PUF slab. Although the detailed flame structure may not be accurately reproduced, it was assumed that the effect of the burner would be negligible if the same HRR and momentum were supplied. To match the momentum of the experimental burner, fresh air was supplied through the burner. Propane was used as the burner fuel because it is a major component of LPG, which was used as the fuel in the experiment. The burner was operated at a constant rate for 120 s, with and additional 10 s of ramp-up before and 10 s of ramp-down after the constant-rate period. Grid sizes of 20, 31.25, 40, and 50 mm were considered. Based on the maximum HRR measured in the experiment, the corresponding PRI values were calculated as 9.7, 6.2, 4.8, and 3.9, respectively. The PUF slab fire simulation conditions were summarized in Table 5.



(a)



(b)

Fig. 4 Dimensions of the PUF slab, based on Pau [6], with unspecified dimensions assumed in this study: (a) Top view and (b) Side view

412 **Table 5.** PUF slab fire simulation conditions.

Variables	Value
PUF Size (m^2)	1×2 [6]
PUF Thickness (mm)	120 [6]
Burner HRR (kW)	25 [6]
Burner operating duration (s)	120
Burner Size (m^2)	1 m × Δx
Fuel	Propane [6]
Grid Size (mm)	20, 31.25, 40, 50

413

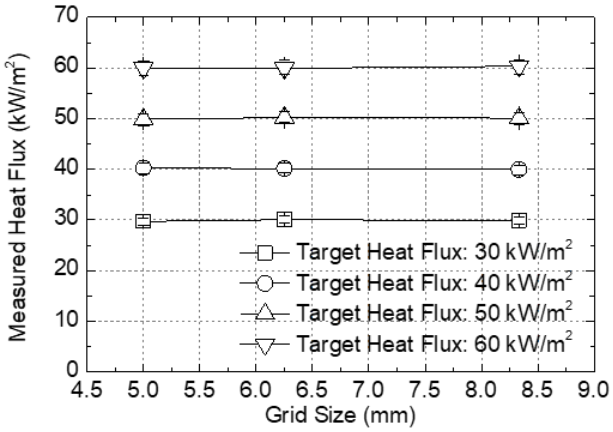
414

4. Results and Discussion

In the first section of the Results and Discussion, the results of the cone calorimeter fire simulations are discussed. First, the accuracy of the cone heater was evaluated, and the basic heat release characteristics of the proposed model were examined. Based on the maximum gas temperatures obtained from the cone calorimeter fire simulations for different grid sizes, the temperatures corresponding to the grid sizes used in the PUF slab fire simulations were extrapolated. These extrapolated temperatures were then used in the grid-independent fire model to determine the thermal properties and a kinetic parameter presented in Table 3. In the second section of the Results and Discussion, the PUF slab fire simulation results are compared with the experimental data for model validation.

4.1 Cone Calorimeter Fire Simulation

Prior to analyzing the cone calorimeter fire simulation results, the coil temperature setting used to achieve the target radiative heat flux was validated. The incident radiative heat flux was measured at 1 cm intervals from the center to 5 cm toward the corner of the specimen. The measured values were averaged for each target heat flux and the grid size, and are presented in Fig. 5. The maximum and minimum incident heat fluxes measured at different locations are presented as error bars. The difference remained below 3% for all measurement conditions, with a maximum difference of 2.7 %.



434

435 **Fig. 5** Measured average radiative heat flux on the specimen

436

437 The heat release rate per unit area (HRRPUA) curves for various grid sizes and external radiative
438 heat fluxes are presented in Fig. 6. The two-stage combustion process was captured by the proposed
439 model. The peak HRR was predicted reasonably well at relatively high external radiative heat fluxes.
440 However, when the external radiative heat flux was low, the peak HRR in the second stage was
441 substantially higher than the experimental result. In this simulation, the surface area exposed to the
442 flame was kept constant for different external radiative heat fluxes. However, the exposed surface area
443 may vary with the external radiative heat flux because of the liquid nature of the polyol [31]. The
444 viscosity of the polyol generally decreases with increasing temperature, allowing the liquid polyol to
445 spread over a wider area. This behavior may be one of the reasons for the variation in the second-stage
446 peak HRR observed in the experiments. In addition, regression of the PUF surface was not reproduced
447 in the simulation, whereas it reduced external radiative heat flux in the experiment. This may have
448 contributed to the higher HRRPUA during the second-stage combustion. As the grid size was reduced,
449 the peak HRRPUA, particularly during the second stage, increased because greater heat feedback to the
450 solid cell adjacent to the flame was predicted with a finer grid. When the grid size was relatively large
451 and the external radiative heat flux was low, the second-stage combustion was not predicted smoothly,
452 resulting in two peaks. This indicates that the sufficient radiative heat flux was not fed back to the

specimen surface to sustain the flame. This is inherent limitation of fire simulations using field model (CFD).

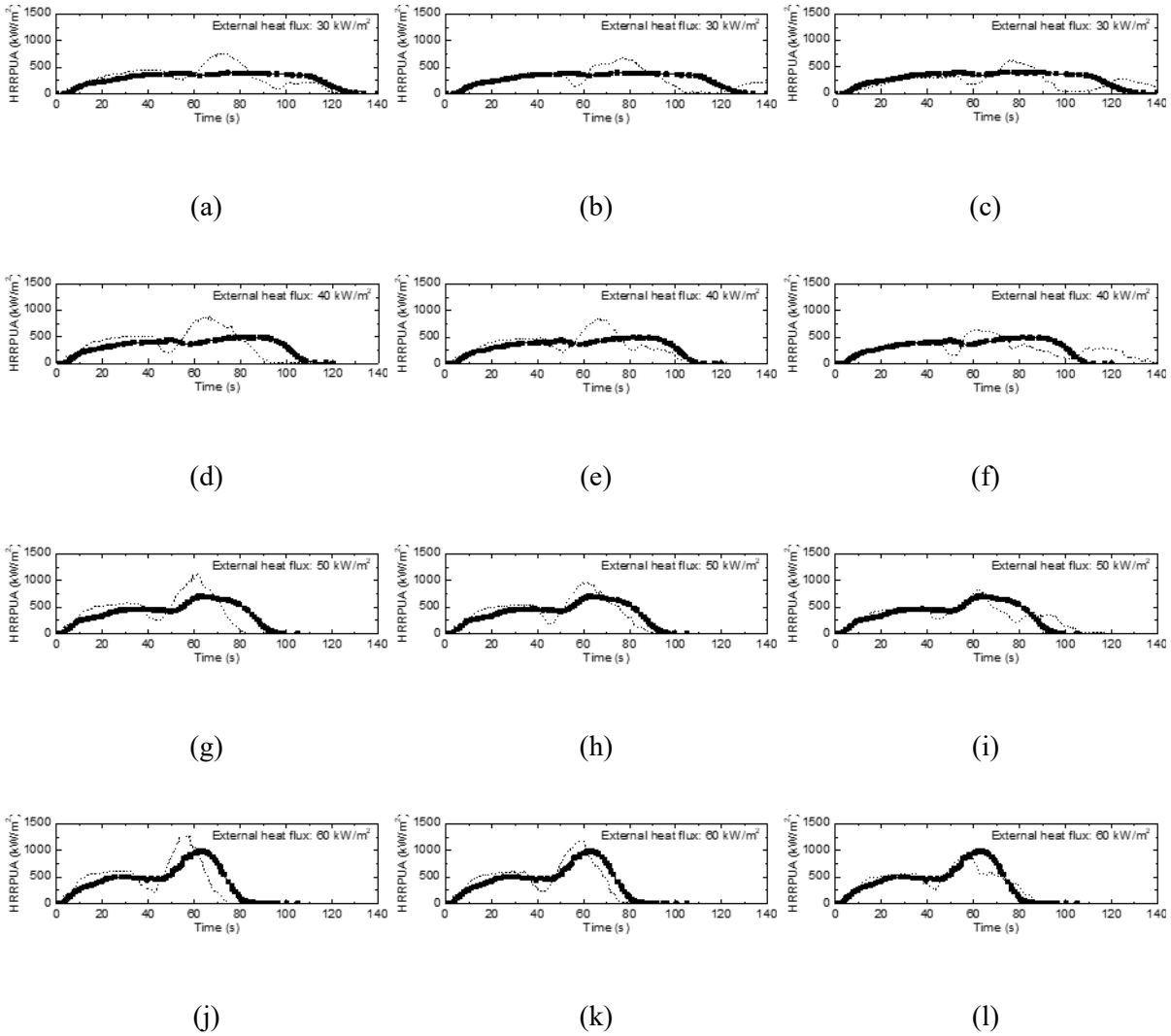


Fig. 6 HRRPUA for various external radiative heat fluxes and grid sizes (solid line with symbols: experiment [6]; dotted line: simulation): (a) Grid size: 5 mm, $\dot{q}_{rad,ex}{}''$: 30 kW/m^2, (b) Grid size: 6.25 mm, $\dot{q}_{rad,ex}{}''$: 30 kW/m^2, (c) Grid size: 8.33 mm, $\dot{q}_{rad,ex}{}''$: 30 kW/m^2, (d) Grid size: 5 mm, $\dot{q}_{rad,ex}{}''$: 40 kW/m^2, (e) Grid size: 6.25 mm, $\dot{q}_{rad,ex}{}''$: 40 kW/m^2, (f) Grid size: 8.33 mm, $\dot{q}_{rad,ex}{}''$: 40 kW/m^2, (g) Grid size: 5 mm, $\dot{q}_{rad,ex}{}''$: 50 kW/m^2, (h) Grid size: 6.25 mm, $\dot{q}_{rad,ex}{}''$: 50 kW/m^2, (i) Grid size: 8.33 mm, $\dot{q}_{rad,ex}{}''$: 50 kW/m^2, (j) Grid size: 5 mm, $\dot{q}_{rad,ex}{}''$: 60 kW/m^2, (k) Grid size: 6.25 mm, $\dot{q}_{rad,ex}{}''$: 60 kW/m^2, and (l) Grid size: 8.33 mm, $\dot{q}_{rad,ex}{}''$: 60 kW/m^2

The proposed model consists of three model components to represent the previously observed vPUF burning process. The mass loss rate of the three components are presented in Fig. 7. As intended, vPUF1,

representing the vPUF that produces low-temperature pyrolysis gases, and vPUF2, representing polyol beads on the vPUF, were pyrolyzed during the first stage of combustion. In contrast, vPUF3, representing the polyol layer formed after the vPUF was exhausted, was pyrolyzed during the second stage of combustion. Although the thermal properties of the polyol beads and the polyol layer are the same, their mass loss rate curves exhibited different characteristics because the used of the 'AREA MULTIPLIER' resulted in different 'THICKNESS' values. This behavior is consistent with the phenomena observed in previous experiments [21, 5, 7, 3].

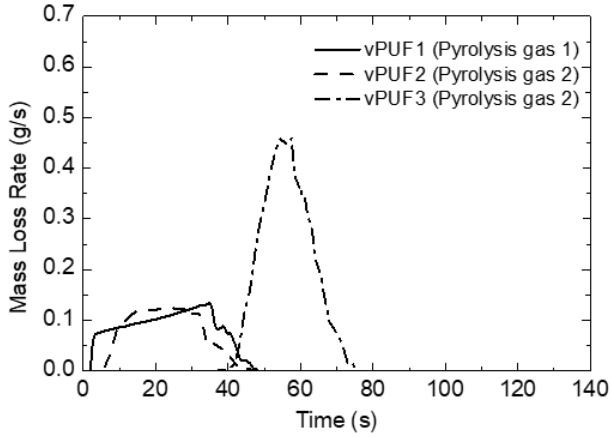
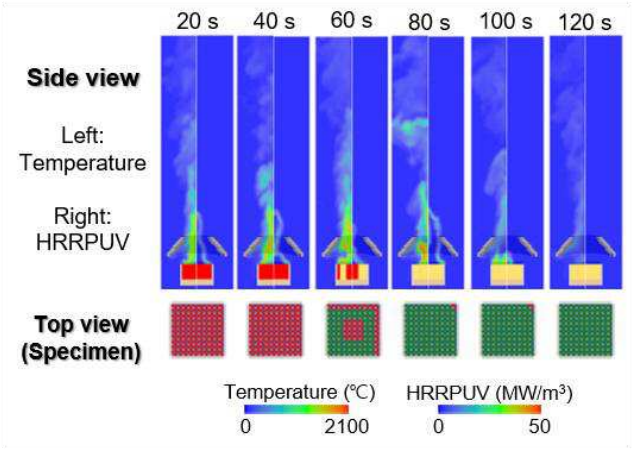


Fig. 7 Mass loss rate of the model components in vPUF (Δx = 5 mm, $\dot{q}_{rad,ext}'' = 60$ kW/m^2)

The combustion process of vPUF using the proposed model is illustrated in Fig. 8. The top view of the specimen is shown at the bottom of the figure. The red surface represents the thermal barrier that prevents vPUF3 from being pyrolyzed during the first stage of combustion. A unit vPUF cell consists of one vPUF1 cell (blue), one vPUF2 cell (gray), and two vPUF3 cells (green) to maintain the number of burning cell within a unit vPUF cell during the first and the second stages of combustion. As shown in the figure, the thermal barrier (red) began to disappear from the high temperature region due to higher pyrolysis rate of vPUF1. Because the unit vPUF cell is not symmetric about its center, the arrangement of the model components across the specimen is also asymmetric. Consequently, the disappearance of

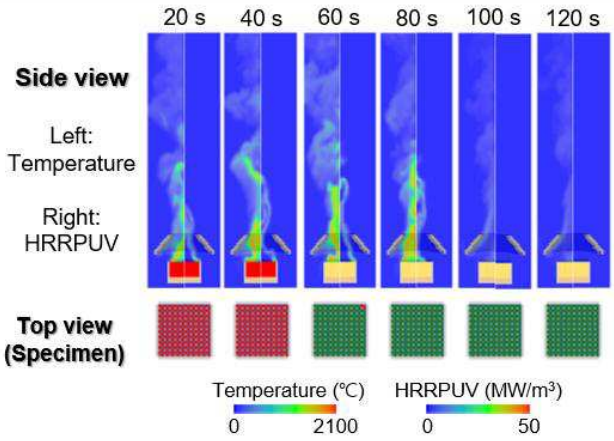
485 the thermal barrier was also asymmetric. Despite the discretization of each vPUF cell into four sub-
486 cells, the fire boundary remained at the specimen boundary. This indicates that the discretization of
487 vPUF had little effect on the predicted fire behavior when a sufficiently fine grid was used.

488



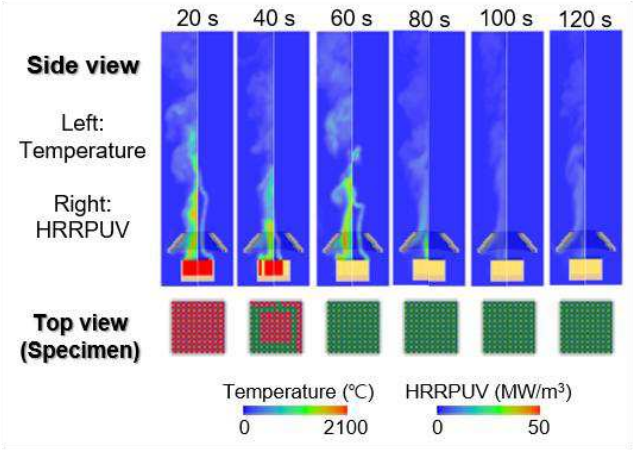
489

490 (a)

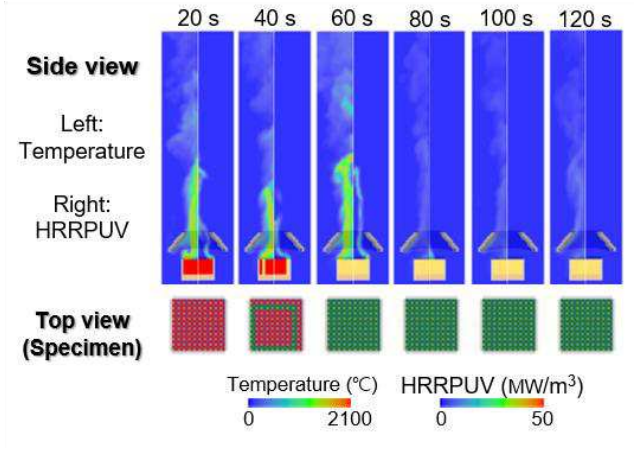


491

492 (b)



(c)



(d)

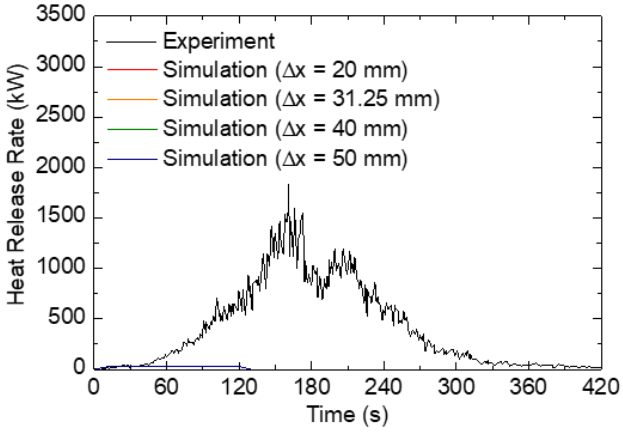
Fig. 8 Combustion process of vPUF for various external radiative heat flux (Δx = 5 mm): External radiative heat fluxes of (a) 30, (b) 40, (c) 50, and (d) 60 kW/m^2

3.2 Polyurethane Foam Slab Fire Simulation

The results of the PUF slab fire simulations using Method 1 are shown in Fig. 9. The initial HRR, which remained constant for 120 s, resulted from the burner being maintained at 25 kW for 120 s. No increase in HRR was observed, indicating that the PUF slabs were not ignited regardless of the grid size. One possible reason for this phenomenon is that the grid sizes used in the PUF slab fire simulations

505 were not sufficiently fine to resolve the flame produced by 25 kW burner, resulting in insufficient heat
506 transfer to the flame-attached solid cells, as explained in Section 2.1. This is a common problem in fire
507 simulations using pyrolysis models, in which the combustible material may fail to ignite or may not
508 burn sufficiently compared with experimental results [14, 6, 3]. To address this problem, the grid-
509 independent fire modeling method described in Section 2.1 was used with method 2 in this study.

510



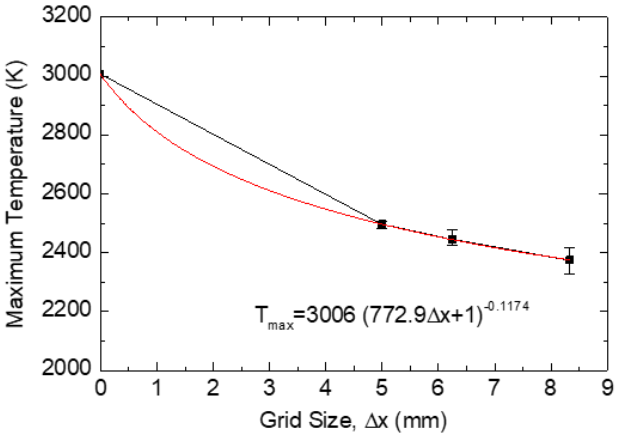
511

512 **Fig. 9** HRR of the PUF slab fire simulation using Method 1 (Experimental data from Pau [6])

513

514 To adopt grid-independent method, the dependence of temperature on the grid size must first be
515 determined. In this study, the maximum gas-phase temperature was obtained from the cone-calorimeter
516 simulations (Fig. 10) and extrapolated to determine the revised activation energy, as presented in Table
517 3. To predict the maximum temperature in the outer region, the equation in the form of $T_{ref}(A \cdot x+1)^b$ was
518 used for fitting. This functional form starts from T_{ref}, which corresponds to the adiabatic flame
519 temperature in this study, and approaches zero as the grid size approaches infinity. This behavior is
520 considered reasonable for extrapolating the temperature in the field model (CFD). Using this equation,
521 the maximum temperatures at the grid sizes of 20, 31.25, 40, and 50 mm were predicted to be 2164,
522 2059, 2002, and 1952 K, respectively.

523



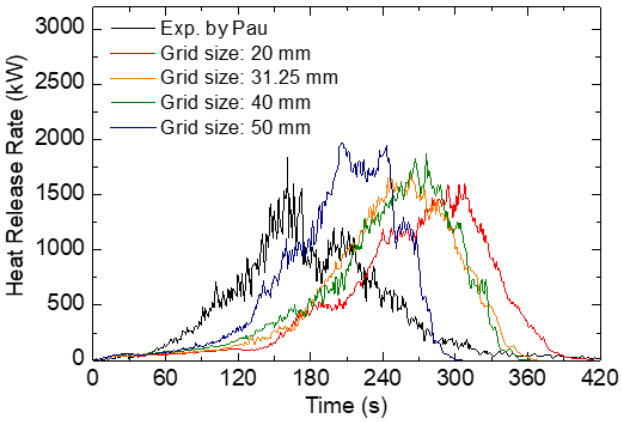
524

525 **Fig. 10** Maximum measured gas temperature in cone calorimeter simulation

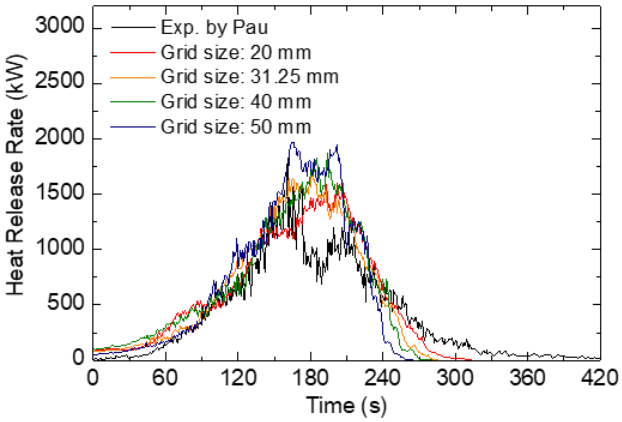
526

527 The PUF fire simulation results for various grid sizes, with the thermal properties and reaction kinetic
528 parameters corrected based on the extrapolated temperature, are shown in Fig. 11 (a). As the grid size
529 increased, the corrected activation energy decreased, facilitating fire spread even under low radiative
530 heat flux. As a result, the case with the 50-mm grid exhibited the fastest ignition, whereas the case with
531 the 20-mm grid exhibited the slowest ignition. Ignition is a complex phenomenon, making it difficult
532 to analyze fire experiment results. Therefore, the results are sometimes normalized by accounting for
533 the time delay and thereby minimizing the effects of ignition [32]. To quantitatively compare the
534 experimental and simulated HRR, the Pearson correlation coefficient, normalized root mean square
535 error (NRMSE), R^2 values were calculated and are presented in Table 6. These values were calculated
536 using the data after accounting for the time delay. The delay was determined by shifting the simulation
537 results in time and identifying the time shift corresponding to the maximum cross-correlation coefficient.
538 As observed in Fig. 11 (a), the delay was shortest for the 50 mm grid and longest for the 20 mm grid.
539 Since the burner HRR was kept constant and the activation energy was reduced most at 50-mm grid,
540 the PUF ignited more readily and exhibited the shortest ignition time. The HRR curves after accounting
541 for the delay are redrawn in Fig. 11 (b). After accounting the delay, the effect of grid size on the HRR
542 was substantially reduced, and the differences between the simulation and experimental results were
543 also reduced. The Pearson correlation coefficients were above 0.9 for all grid sizes, the NRMSE values

remained below 0.13, and R^2 values were above 0.6. These results indicate that the simulations captured the overall growth and decay trends well, although slight differences remained between the simulated and experimental HRR values at individual time points.



(a)



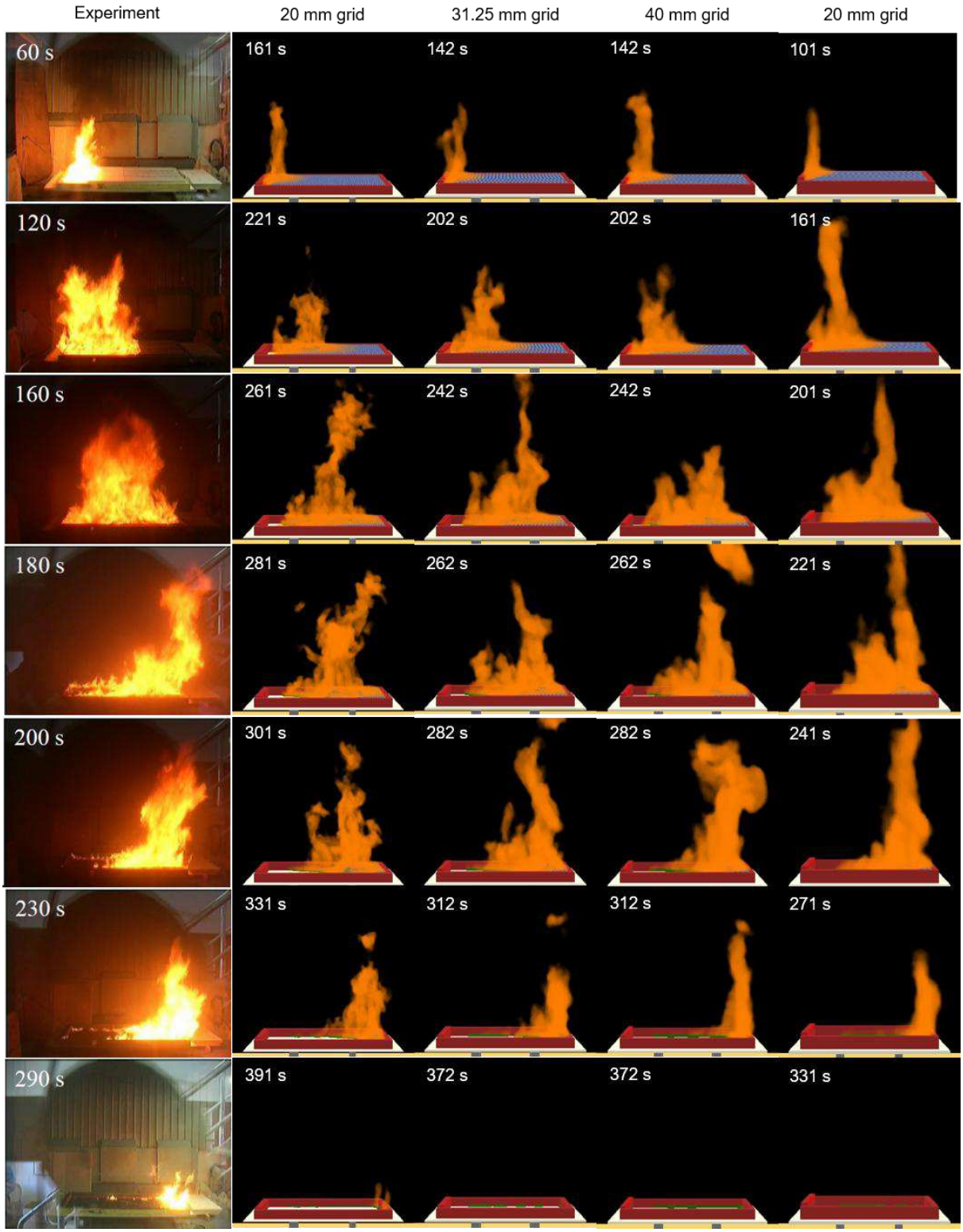
(b)

Fig. 11 HRR of the PUF slab fire simulation using Method 2 (Experimental data from Pau [6]): (a) HRR comparison without adjusting time delay and (b) HRR comparison with adjusting time delay

Table 6. Quantitative comparison of PUF slab fire simulation with experimental data.

	Grid size (mm)			
	20	31.25	40	50
Delay (s)	101	82	82	41
Pearson correlation coefficient	0.9491	0.9599	0.9342	0.9296
NRMSE	0.0823	0.0866	0.1053	0.1289
R-square	0.8441	0.8276	0.7448	0.6177

The experimental fire images obtained by Pau [6] and the corresponding simulation fire images, defined by regions with HRRPUV values above 200 kW/m^3, are compared in Fig. 12 accounting for the time delays described in Table 6. The scale of the simulation images was adjusted to match that of experimental images. Some simulation images showed different flame lengths compared with the experimental images. For example, the flame length predicted using the 50 mm grid at 161 s was much longer than that observed in the experiment. The flame length varies due to the inherently turbulent nature of flames; therefore, the flame length obtained from the simulation cannot be directly compared with the experimental data. However, the burning area predicted by the simulation showed very similar results to those observed in the experiment. For example, the burning area of the PUF slab at 120 s in experiment was approximately half of the total slab area, which was also observed in the simulation at the corresponding time. After 160 s, the burning area spread over entire PUF slab, and the same behavior was observed in the simulation results. The grid-independent model using PUF fire modeling Method 2 showed consistent results when the ignition-induced delay was accounted for.



572

573 **Fig. 12** Fire growth and decay comparison between simulation and experiment (Experimental data

574 from Pau [6])

The quantitative data predicted by the simulation are compared with the experimental results in Table 7. The quantities used for this comparison were based on the data presented by Pau [6], and the same definition were used. The average mass loss rate ($\dot{m}_{ave}$) was calculated over the period during which the burned mass ranged from 10 % to 90 % of the total burned mass. The total heat release (q_{tot}) was calculated by including the heat release from the burner. The effective heat of combustion ($\Delta h_{c,eff}$) was calculated over the entire experimental period. However, Pau [6] did not specify whether the heat release from the propane burner was included in the calculation of the total heat release. Therefore, the burner heat release was considered in $\Delta h_{c,eff}$ calculation, consistent with the calculation of the total heat release. The peak heat release rate ($\dot{q}_{pk}$) was determined as the maximum value during the combustion period. The average heat release rate ($\dot{q}_{ave}$) was calculated over the period during which the HRR exceeded 10 % of its maximum value. The maximum error was observed for $\dot{q}_{ave}$ at the 50-mm grid size, reaching 53.9 %. This was attributed to the relatively high $\dot{q}_{pk}$ and short burning period in this case. Except for this case, all the errors remained below 30 %. The errors for $\Delta h_{c,eff}$ were the lowest among the evaluated quantities because it was directly specified as an input parameter in the simulation. In contrast, the error for $\dot{q}_{ave}$ was the highest because it depends on the other quantities presented above. Since the grid-independent fire modeling method was used, no clear trend in the errors with respect to grid size was observed.

Table 7. Errors in major quantitative results of PUF slab fire simulation (Experimental data from Pau [6]).

	$\dot{m}_{ave}(g/s)$	$q_{tot}(MJ)$	$\Delta h_{c,eff}(MJ/kg)$	$\dot{q}_{pk}(kW)$	$\dot{q}_{ave}(kW)$
Exp. [6]	39.2	166.5	25.3	1834	712
Sim. (Δx=20mm)	38.5 (-1.8 %)	196.6 (18.1 %)	27.3 (7.9 %)	1604 (-12.5 %)	821 (15.3 %)
Sim. (Δx=31.25mm)	40.1 (2.3 %)	196.5 (18.0 %)	27.3 (7.9 %)	1638 (-10.7 %)	870 (22.2 %)

Sim. (Δx=40mm)	42.3 (7.9 %)	201.0 (20.7 %)	27.3 (7.9 %)	1884 (2.7 %)	903 (26.8 %)
Sim. (Δx=50mm)	50.7 (29.3 %)	200.7 (20.5 %)	27.3 (7.9 %)	2166 (18.1 %)	1096 (53.9 %)

596

597 The total mass burned in the simulation is summarized in Table 8. Approximately 96-99 % of the
598 total mass was burned in the simulations. The unburned cells were mainly located near the support
599 bracing. Although the grid-independent fire modeling method was used, the size of the turbulent
600 vortices that can be directly resolved is limited by the grid size, which can affect convective heat transfer
601 near the wall. In addition, heat loss to adjacent solid cells can contribute to cessation of burning.

602

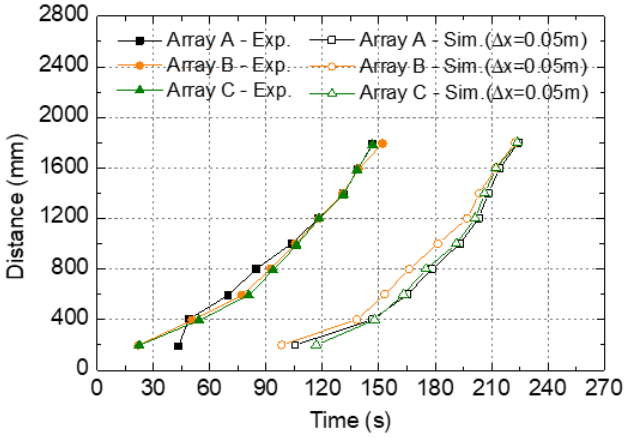
603 **Table 8.** Total mass burned for various grid sizes.

Grid size (mm)	Total mass burned (kg)
20	7.2 (96.8 %)
31.25	7.2 (96.8 %)
40	7.37 (99.1 %)
50	7.36 (98.9 %)

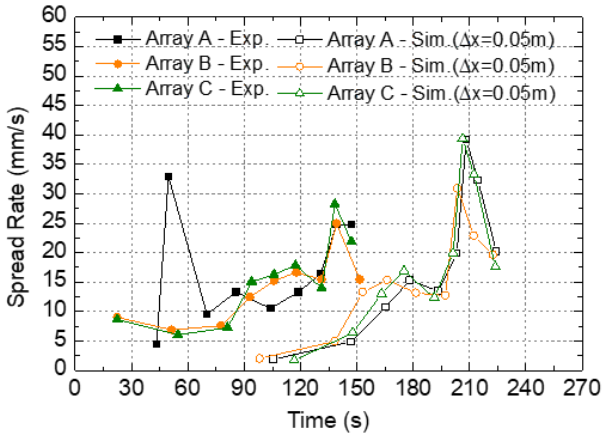
604

605 Lastly, fire spread characteristics over the slab was analyzed. In the experiment, the pyrolysis front
606 was identified based on a temperature of 222 ℃, which was determined to be the onset temperature of
607 pyrolysis. In the grid-independent fire modeling method, the gas-phase temperature assumed to
608 decrease as the grid size increased. Based on this assumption, the activation energy was corrected
609 accordingly. Therefore, using 495 K (222 ℃) as the reference temperature, the temperature for
610 identifying the pyrolysis front, the corresponding temperature for different grid sizes were determined
611 in proportion to the temperatures predicted by the equation in Fig. 10. Using these temperatures, the
612 distance traveled by the pyrolysis front and the fire spread rate, defined as the derivative of the pyrolysis
613 front travel distance, were calculated and are presented in Fig. 13. As a representative case, the
614 simulation results for the 50-mm grid were selected because it is the largest grid size considered in this
615 study. This case demonstrates that the grid-independent fire modeling method can also be applied to
616 building-scale fire simulations using relatively coarse grids. The distance traveled by the pyrolysis front

predicted by the simulation showed a similar trend to that observed in the experiment, except for a time delay. The fire spread rate, defined as the derivative of the distance traveled by the pyrolysis front, also exhibited a similar trend: it was relatively low during the initial period and increased as the fuel consumed. During the middle period, the fire spread rate showed similar values, remaining approximately 15 mm/s at 110 s in the experiment and 170 s in the simulation. In addition, a sudden increase in the fire spread rate near the end of the burning period was captured at 140 s in the experiment and 210 s in the simulation. However, the fire spread rate predicted by the simulation was approximately 1.6 times higher than that measured in the experiment.



(a)



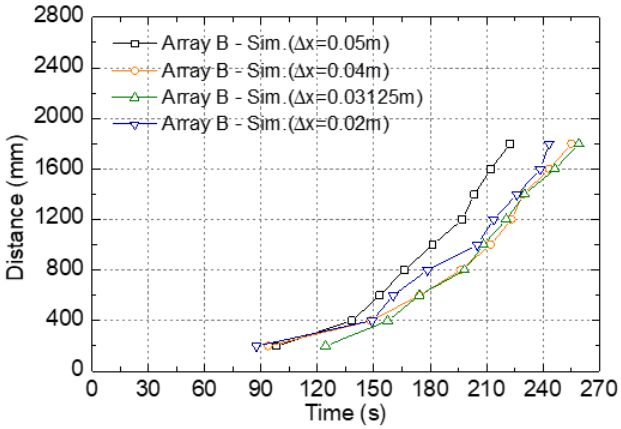
(b)

630 **Fig. 13** Comparison of fire spread characteristics between simulation (Δx=0.05 m) and experiment
631 (Experimental data from Pau [6]): (a) Distance traveled by the pyrolysis front and (b) Fire spread rate

632

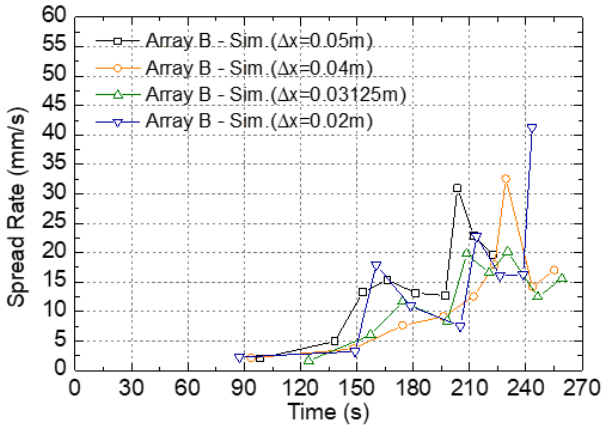
633 The distance traveled by the pyrolysis front and the corresponding fire spread rate measured by TC
634 array B (at the center of the PUF slab) are shown in Fig. 14. The pyrolysis front distance and average
635 slope showed similar trends for various grid sizes, except for a time delay. The fire spread rate fluctuated
636 during the burning period; however, it generally increased as the fuel was consumed. The variation with
637 respect to grid size was much smaller than the fluctuation in the fire spread rate. These results indicate
638 that the grid-independent fire modeling method combined with the pyrolysis-based fire modeling can
639 be applied using a coarse grid, provided that the time delay is appropriately corrected.

640



641

642 (a)



643

644 (b)

645 **Fig. 14** Comparison of fire spread characteristics depending on the grid sizes (Array B): (a)

646 Distance traveled by the pyrolysis front and (b) Fire spread rate

5. Conclusions

In this study, a PUF fire modeling method was proposed in combination with a grid-independent fire modeling method to enable fire simulations using coarse grid. The proposed PUF fire model was validated against cone calorimeter experiments, and a PUF slab fire was simulated using the grid-independent fire modeling method. The major findings of this study are summarized as follows:

(1) A proposed PUF fire model reproduced the two-stage combustion behavior of PUF observed in the cone calorimeter experiments. At higher external radiative heat fluxes, the peak HRRPUA values in both the first and second stages were well captured. At lower external radiative heat fluxes, however, the peak HRRPUA in the second stage was higher than that observed in the experiment.

(2) The proposed PUF fire model predicted the pyrolysis of each modeling component selected based on the observations of PUF fire behavior and showed a smooth transition from the first to the second combustion stage. However, asymmetric disappearance of the thermal barrier, particularly near the edge of the specimen, was observed due to the asymmetric arrangement of the unit PUF cells.

(3) The maximum temperature obtained from the cone calorimeter simulations was used to derive an equation for estimating the gas-phase temperature as a function of grid size. The temperature for the coarse grid was extrapolated using the derived equation and applied to the grid-independent fire modeling method. The grid-independent fire model successfully ignited and simulated the spread the PUF slab fire in all grid sizes considered in this study, whereas the PUF fire model alone was unable to ignite the PUF slab.

(4) The HRR showed similar characteristics across the different grid sizes, except for a time delay. In addition, the pyrolysis front distance and its derivative, i.e., the fire spread rate, showed similar trends to the experimental results and exhibited little variation with grid size. These results indicate the proposed grid-independent fire modeling method can be applied using coarse grids, provided that the time delay is appropriately corrected.

673 **Acknowledgments**

674 This research was supported by Seoul National University of Science and Technology.

Author Contributions

Taehoon Kim: Conceptualization, Data curation, Methodology, Validation, Formal analysis, Investigation, Visualization, Writing – Original draft, Writing – review and Editing

Declarations

Conflict of Interests

The author has no relevant financial or non-financial interests to disclose.

References

1. Chen Y, Guo X, Zhang J, Zhao Y, Zhong T, Zhang Y. Experimental study on flame spread characteristics over discrete U-shaped building insulation foam and the fire blocking mechanism of fire barrier. Fire Saf J. 2026;165:104943. doi:https://doi.org/10.1016/j.firesaf.2026.104943.

2. Hamins A, Di Cristina G, Bundy M, Kim I, Zammarano M. Fire performance of mattresses with contemporary bedding materials. Fire Saf J. 2026;162:104695. doi:https://doi.org/10.1016/j.firesaf.2026.104695.

3. Prasad K, Kramer R, Marsh N, Nyden M, Ohlemiller T, Pitts W et al., editors. Numerial simulation of fire spread on polyurethane foam slabs. Fire and Materials Conference; 2009 2009-03-17; San Francisco, CA: Proceedings of the Fire and Materials Conference, San Francisco, CA.

4. McKeen P, Liao Z. Pyrolysis model for predicting the fire behavior of flexible polyurethane foam. Build Simul. 2019;12(2):337-45. doi:10.1007/s12273-018-0484-2.

5. Chen Y, He H, Liu Z. Numerical modeling of flexible polyurethane foam combustion under two ignition modes. Fuel. 2022;309:122204. doi:https://doi.org/10.1016/j.fuel.2021.122204.

6. Pau D. A comparative study on combustion behaviours of polyurethane foams with numerical simulations using pyrolysis models [Ph D Dissertation]: University of Canterbury; 2013.

7. Pitts WM. Role of two stage pyrolysis in fire growth on flexible polyurethane foam slabs. Fire Mater. 2014;38(3):323-38. doi:https://doi.org/10.1002/fam.2183.

8. Mangs J, Hostikka S. Experiments and numerical simulations of vertical flame spread on charring materials at different ambient temperatures. Fire Saf Sci. 2011;10:499-512. doi:10.3801/IAFSS.FSS.10-499.

9. Xu Q, Hofmeyer H, Maljaars J, van Herpen RAP. Pyrolysis modelling of insulation material in coupled fire-structure simulations. J Build Eng. 2024;98:110969. doi:https://doi.org/10.1016/j.jobe.2024.110969.

10. Kim T. Modeling of wood crib fires using a detailed pyrolysis model. Therm Sci Eng Prog. 2024;47:102339. doi:https://doi.org/10.1016/j.tsep.2023.102339.

11. Feng H, Zhou X, Cong B. Simulation study on flame characteristics and heat transfer mechanisms of a rectangular fire source attached to a pyrolysis wall. Int J Therm Sci. 2025;217:110083. doi:https://doi.org/10.1016/j.ijthermalsci.2025.110083.

12. Dréan V, Girardin B, Guillaume E, Fateh T. Numerical simulation of the fire behaviour of facade equipped with aluminium composite material-based claddings-Model validation at large scale. Fire Mater. 2019;43(8):981-1002. doi:https://doi.org/10.1002/fam.2759.

13. Cui Z, Chun Q, Song H. Research on the multi-scale combustion performance of timber structures considering fungal decay: From material pyrolysis to building fire dynamics. Case Stud Constr Mater. 2026;25:e06482. doi:https://doi.org/10.1016/j.cscm.2026.e06482.

14. Wang X, Fleischmann C, Spearpoint M. Applying the FDS pyrolysis model to predict heat release rate in small-scale forced ventilation tunnel experiments. Fire Saf J. 2020;112:102946. doi:https://doi.org/10.1016/j.firesaf.2020.102946.

15. Maragkos G, Merci B. Large Eddy Simulations of CH4 Fire Plumes. Flow Turbul Combust. 2017;99(1):239-78. doi:10.1007/s10494-017-9803-4.

16. Abani N, Kokjohn S, Park SW, Bergin M, Munnannur A, Ning W et al. An Improved Spray Model for Reducing Numerical Parameter Dependencies in Diesel Engine CFD Simulations. SAE World Congress & Exhibition; Aprill 14, 2008; Detroit, Michigan, United States: SAE International; 2008.

17. Dehghani P, Chaudhari DM, DiDomizio MJ, Floyd JE. Toward grid-independent modeling of natural convection with fire dynamics simulator. Inte J Heat Mass Transf. 2025;250:127190. doi:https://doi.org/10.1016/j.ijheatmasstransfer.2025.127190.

18. Garrido MA, Font R. Pyrolysis and combustion study of flexible polyurethane foam. J Anal Appl Pyrolysis. 2015;113:202-15. doi:https://doi.org/10.1016/j.jaap.2014.12.017.

19. Chao CYH, Wang JH. Comparison of the Thermal Decomposition Behavior of a Non-Fire Retarded and a Fire Retarded Flexible Polyurethane Foam with Phosphorus and Brominated Additives. J Fire Sci. 2001;19(2):137-56. doi:10.1106/q56w-kudb-0vrt-6hlf.

20. Day M, Cooney JD, MacKinnon M. Degradation of contaminated plastics: a kinetic study. Polym Degrad Stab. 1995;48(3):341-9. doi:https://doi.org/10.1016/0141-3910(95)00088-4.

734 21. Krämer RH, Zammarano M, Linteris GT, Gedde UW, Gilman JW. Heat release and structural
735 collapse of flexible polyurethane foam. Polym Degrad Stab. 2010;95(6):1115-22.
736 doi:https://doi.org/10.1016/j.polymdegradstab.2010.02.019.
737 22. Pau D, Fleischmann C, Delichatsios M. Apparatus for investigating the burning and dripping of
738 vertically oriented polyurethane foams. Fire Mater. 2020;44(2):211-29.
739 doi:https://doi.org/10.1002/fam.2794.
740 23. Liu Z, He H, Zhang J, Zheng J, Zhuang H. Experimental investigation and numerical simulation of
741 the combustion of flexible polyurethane foam with larger geometries. Polym Test. 2020;81:106270.
742 doi:https://doi.org/10.1016/j.polymertesting.2019.106270.
743 24. Pau DSW, Fleischmann CM, Spearpoint MJ, Li KY. Thermophysical properties of polyurethane
744 foams and their melts. Fire Mater. 2014;38(4):433-50. doi:https://doi.org/10.1002/fam.2188.
745 25. Pau DSW, Fleischmann CM, Spearpoint MJ, Li KY. Determination of kinetic properties of
746 polyurethane foam decomposition for pyrolysis modelling. J Fire Sci. 2013;31(4):356-84.
747 doi:10.1177/0734904113475858.
748 26. Friedman HL. New methods for evaluating kinetic parameters from thermal analysis data. J Polym
749 Sci, Part B, Polym Lett. 1969;7(1):41-6. doi:https://doi.org/10.1002/pol.1969.110070109.
750 27. Ahmed MM, Trouvé A. Large eddy simulation of the unstable flame structure and gas-to-liquid
751 thermal feedback in a medium-scale methanol pool fire. Combust Flame. 2021;225:237-54.
752 doi:https://doi.org/10.1016/j.combustflame.2020.10.055.
753 28. Babrauskas V. The Cone Calorimeter. In: Hurley MJ, Gottuk D, Hall JR, Harada K, Kuligowski E,
754 Puchovsky M et al., editors. SFPE Handbook of Fire Protection Engineering. New York, NY: Springer
755 New York; 2016. p. 952-80.
756 29. McGrattan K, Hostikka S, Floyd J, McDermott R, Vanella M, Mueller E. Fire Dynamics Simulator
757 Technical Reference Guide Volume 3: Validation. National Institute of Standards and Technology,
758 Building and Fire Research …; 2024.
759 30. McGrattan K, Floyd J, Forney G, Baum H, Hostikka S, editors. Improved Radiation and Combustion
760 Routines for a Large Eddy Simulation Fire Model2005 2005-06-16: Fire Safety Science. Proceedings.

761 Seventh (7th) International Symposium. International Association for Fire Safety Science (IAFSS),
762 Boston, MA; Fire Safety Science. Proceedings. Seventh (7th) International Symposium. International
763 Association for Fire Safety Science (IAFSS), Boston, MA.
764 31. McKeen P, Liao Z. A three-layer macro-scale model for simulating the combustion of PPUF in
765 CFD. Build Simul. 2016;9(5):583-96. doi:10.1007/s12273-016-0287-2.
766 32. Wilkens Flecknoe-Brown K, van Hees P. Geometrical and environmental effect on fire behaviour
767 of polyurethane foam slabs. Fire Mater. 2023;47(7):892-909. doi:https://doi.org/10.1002/fam.3133.

768